Journal of Theoretical and Applied Information Technology
31st May 2013. Vol. 51 No.3

ISSN: 1992-8645 www.jatit.org E-ISSN: 1817-3195

A SPHERICAL ELECTROSTATIC MODEL EDGE DETECTOR FOR OMNIDIRECTIONAL IMAGES

[1] OMAR EL KADMIRI, [2] ZAKARIA EL KADMIRI, [3] LHOUSSAINE MASMOUDI

[1, 2]PhD. Std, LETS/Geomat Laboratory, Physics Dept. Faculty of Science, Mohammed V University-Agdal, Morocco

[3]Prof, LETS/Geomat Laboratory, Physics Dept. Faculty of Science, Mohammed V University-Agdal, Morocco

E-mail: [1]omar.elkadmiri@gmail.com, [2]zakariaelkadmiri@gmail.com, [3]masmoudi@fsr.ac.ma

ABSTRACT

Recently, omnidirectional vision has become necessary and useful for many computer science applications, such as autonomous navigation, SLAM, video surveillance and conferencing. However the use of classical image processing tools for omnidirectional images without taking into account their special particularities leads to a lack of performance. This article presents a new gray level edge detector based on a spherical virtual electrostatic model more appropriate for omnidirectional images. Several experimental results are given to illustrate the potential of this non-gradient based approach on various images especially against noise. Confrontation to other classical methods is provided.

Keywords: *Edge detection, Omnidirectional images, Electrostatic charges model, Stereographic projection, Fram & Deutsch.*

1. INTRODUCTION

One of the main advantages of omnidirectional vision is its ability to enhance the field of view (FOV) to cover 360° of the surrounding scene unlike classical cameras which have a limited field of view. To enhance this one many technics have been designed and used in the literature [1-9].

All omnidirectional vision sensors have some advantages and limitations. Depending on the application, a compromise has to be made between high resolution images and real time processing or video rate. Among all ways to enlarge the field of view, the catadioptric system is one of the most frequently used to acquire omnidirectional images. This imaging system is based on a combination of a convex mirror-lens and a camera, which leads to a catadioptric vision system providing a full 360° field of view.

Catadioptric cameras have been widely studied, since Nayar [10] reported in 1997 the catadioptric camera with single view point SVP. More researches have been done later in this field [11-24]. These sensors were proven useful in many applications such as surveillance [25], navigation [26], localization [27], and simultaneous localization and mapping SLAM [28].

However, these catadioptric systems have the drawback to generate radial distortions on the acquired images due to the geometrical properties of sensors. Consequently the classical image processing tools, such as edge detection operators, segmentation algorithms, smoothing and morphological operators, are unsuitable for this kind of images.

Edge detection is an indispensable tool in image processing, machine and computer vision, especially in the field of feature detection and extraction, which consist of identifying rapid variation in some physical properties, such as geometry, gray-level values, and reflectivity.

The aim of detecting sharp variation in image brightness is to detect important events and changes in scene properties. It can be proved that under fairly general assumptions for an image formation model, image brightness discontinuities correspond to depth, or surface orientation discontinuities, changes in material properties, or in scene illumination.

Often classical image processing tools for planar images are applied directly on omnidirectional ones. Nevertheless, these techniques are not really geometrically adapted to this kind of images because they consider the image as a uniform space, without taking into account image distortions introduced by catadioptric sensors.

Some interesting research studies tried to adapt conventional image processing tools to omnidirectional images while taking into

Journal of Theoretical and Applied Information Technology
31st May 2013. Vol. 51 No.3

ISSN: 1992-8645 www.jatit.org E-ISSN: 1817-3195

consideration there particularities. In [29] a SIFT (Scale Invariant Feature Transform) in the spherical coordinates for omnidirectional images was proposed, conducted experiments in this study are confirming the promising and accurate performance of such algorithms. And authors of [30] have proposed an edge detector adapted to omnidirectional image geometry, with Fuzzy sets used to take into account all imprecisions introduced by the sampling process allowing a coherent edge detection on omnidirectional images.

So it is more interesting to develop an edge detection method directly on the spherical space which is suitable for omnidirectional images and leads to better results. In [31] we have proposed an electrostatic model edge detector for planar images. The approach has proved its performance confronting gradient-based methods. Hence, we developed a new gray level edge detector based on a spherical virtual electrostatic model. The approach will be detailed in section 2, and section 3 describes the stereographic projection algorithm used to perform the proposed approach. Experimental results, evaluations and confrontation to other edge operators are given in section 4.

2. AN EDGE DETECTION OPERATOR BASED ON A SPHERICAL VIRTUAL ELECTROSTATIC CHARGES DISTRIBUTION

The omnidirectional image can be modeled as a spherical grid of charged particles distributed on a spherical surface in electrostatic equilibrium.

The image is split into 3 x 3 pixels blocks (see Fig. 1). We suppose that forces exerted by charges beyond the 3x3 window on the central charge are neglected. The following analogy is made: the pixels intensity corresponds to electric charges, and the central charge is subjected to the electrostatic forces of the eight neighboring charges. The electric forces components could be calculated by equation (3). We distinguish between two kinds of forces: attractive and repulsive ones. According to the electrostatic equilibrium condition, we have:

$$\sum_{i=1}^{n} \overrightarrow{F_i} = 0$$

Consider two electric charges q_0 and q_1 separated with a distance r. there is an electrostatic field between these two fixed charges. The charge q_1 generates an electrostatic field $\overrightarrow{E_1}$:

$$\overrightarrow{E_1} = \frac{q_1}{4\pi\varepsilon_0}\frac{\vec{r}}{r^3} \qquad (1)$$

The mutual forces exerted by the field $\overrightarrow{E_1}$ on q_0 is $\vec{F}\, q_1/q_0$ according to coulomb's law this force is given by:

$$\vec{F}\, q_1/q_0 = q_1\overrightarrow{E_1} = q_1 \frac{q_0}{4\pi\varepsilon_0}\frac{\vec{r}}{r^3} \qquad (2)$$

$$\vec{F}\, q_1/q_0 = kq_1q_0\frac{\vec{r}}{r^3} \qquad (3)$$

Where $k = \frac{1}{4\pi\varepsilon_0}$

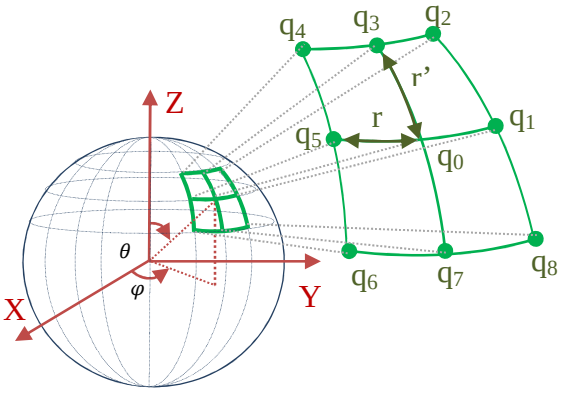

Figure 1. Distribution of electric charges on the sphere.

Attractive Forces:

In a spherical reference $R\,(o, \vec{e}_r, \vec{e}_\varphi, \overrightarrow{e_\theta})$, the charges q_i where $i = 1,2,\ldots,8$ exercise attractive forces on the charge q_0 which have an opposite charge.

Let $\overrightarrow{T_\varphi}$ and $\overrightarrow{L_\theta}$ respectively, the forces exerted on q_0 toward $\vec{e}_\varphi$ et $\overrightarrow{e_\theta}$:

$$\overrightarrow{T_\varphi} = \vec{F}\, q_1/q_0 + \vec{F}\, q_5/q_0 = k\,\frac{q_0}{r^2}(q_5 - q_1)\,\vec{e}_\varphi$$

$$\overrightarrow{L_\varphi} = \vec{F}\, q_3/q_0 + \vec{F}\, q_7/q_0 = k\,\frac{q_0}{r'^2}(q_3 - q_7)\overrightarrow{e_\theta}$$

Where $r = Rsin\theta d\varphi$; $r' = r$

$$\overrightarrow{T_\varphi} = k\,\frac{q_0}{(Rsin\theta d\varphi)^2}(q_5 - q_1)\,\vec{e}_\varphi \qquad (4)$$

$$\overrightarrow{L_\varphi} = k\,\frac{q_0}{(Rsin\theta d\varphi)^2}(q_3 - q_7)\overrightarrow{e_\theta} \qquad (5)$$

For the diagonal forces we have:

$$\vec{F}D_1 = \vec{F}\, q_2/q_0 + \vec{F}\, q_6/q_0 = k\,\frac{q_0}{\delta^2}(q_6 - q_2)\,\vec{D}_1$$

$$\vec{F}D_2 = \vec{F}\, q_8/q_0 + \vec{F}\, q_4/q_0 = k\,\frac{q_0}{\delta^2}(q_4 - q_8)\,\vec{D}_2$$

Journal of Theoretical and Applied Information Technology
31st May 2013. Vol. 51 No.3

ISSN: 1992-8645 www.jatit.org E-ISSN: 1817-3195

$$\overrightarrow{D_1} = cos(\lambda)\,\vec{e}_\varphi - sin(\lambda)\overrightarrow{e_\theta}$$

$$\overrightarrow{D_2} = cos(\lambda)\,\vec{e}_\varphi + sin(\lambda)\overrightarrow{e_\theta}$$

Where $\lambda=\pi/4$ and $\delta^2 = 2r^2 = 2(Rsin\theta d\varphi)^2$

The diagonal forces expressions become:

$$\vec{F}D_1 = k\,\frac{q_0\sqrt{2}}{4(Rsin\theta d\varphi)^2}(q_6 - q_2)(\overrightarrow{e_\varphi} - \overrightarrow{e_\theta}) \quad (6)$$

$$\vec{F}D_2 = k\,\frac{q_0\sqrt{2}}{4(Rsin\theta d\varphi)^2}(q_4 - q_{82})(\overrightarrow{e_\varphi} + \overrightarrow{e_\theta}) \quad (7)$$

Let $k' = k / R^2$

And $\overrightarrow{F_\varphi} = F_\varphi\overrightarrow{e_\varphi}$ $\overrightarrow{F_\theta} = F_\theta\overrightarrow{e_\theta}$

The equations (4), (5), (6), (7) become:

$$\overrightarrow{T_\varphi} = k'\,\frac{q_0}{(sin(\theta)d\varphi)^2}(q_5 - q_1)\,\vec{e}_\varphi$$

$$\overrightarrow{L_\varphi} = k'\,\frac{q_0}{(sin(\theta)d\varphi)^2}(q_3 - q_7)\overrightarrow{e_\theta}$$

$$\vec{F}D_1 = k'\,\frac{q_0\sqrt{2}}{4(sin(\theta)d\varphi)^2}(q_6 - q_2)(\overrightarrow{e_\varphi} - \overrightarrow{e_\theta})$$

$$\vec{F}D_2 = k'\,\frac{q_0\sqrt{2}}{4(sin(\theta)d\varphi)^2}(q_4 - q_{82})(\overrightarrow{e_\varphi} + \overrightarrow{e_\theta})$$

Finely

$$\overrightarrow{F_\varphi} = k'q_0\,\frac{1}{(sin(\theta)d\varphi)^2}[q_5 - q_1 + \frac{\sqrt{2}}{4}(q_6 - q_2 + q_4 - q_8)]\,\vec{e}_\varphi \quad (8)$$

$$\overrightarrow{F_\theta} = k'q_0\,\frac{1}{(sin(\theta)d\varphi)^2}[q_3 - q_7 + \frac{\sqrt{2}}{4}(q_2 - q_6 + q_4 - q_8)]\,\overrightarrow{e_\theta} \quad (9)$$

If $p(i,j) = q_0$ is the central pixel defined on the studied block, we obtain the two filters G_φ et G_θ toward φ and θ directions defined as:

$$G_\varphi = 1/(sin(\theta)\,d\varphi)^2 \begin{pmatrix} \sqrt{2}/4 & 0 & -\sqrt{2}/4 \\ 1 & 0 & -1 \\ \sqrt{2}/4 & 0 & -\sqrt{2}/4 \end{pmatrix} \quad (10)$$

and

$$G_\theta = 1/(sin(\theta)\,d\varphi)^2 \begin{pmatrix} \sqrt{2}/4 & 1 & \sqrt{2}/4 \\ 0 & 0 & 0 \\ -\sqrt{2}/4 & -1 & -\sqrt{2}/4 \end{pmatrix} \quad (11)$$

3. AN EDGE DETECTION ALGORITHM FOR OMNIDIRECTIONAL IMAGES

It is well known that omnidirectional images are not uniformly sampled; the amount of information contained in each pixel in not the same, more near is the pixel to the center, greater is the amount of information it contains.

Conventional filters designed for planar images do not take into account the real neighbors of each processed pixel during their application to an omnidirectional image. This fact is well illustrated in Figure 2 which shows how planar and spherical filters convolute an omnidirectional image.

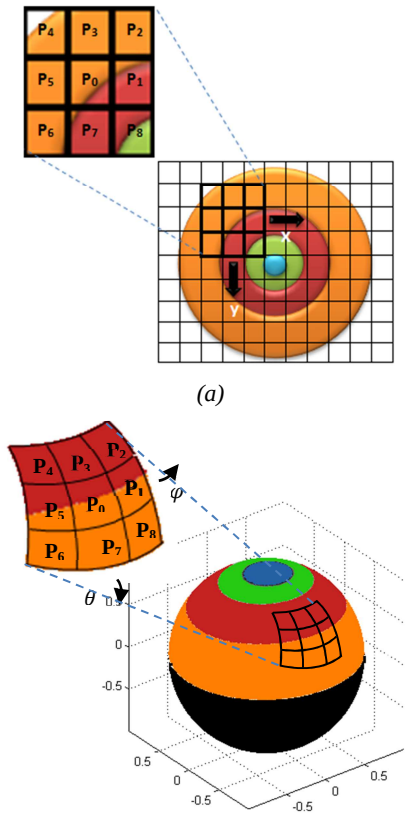

Figure 2. (a): illustration of false neighboring pixels in the case of planar filters. (b): True neighboring pixels in the case of spherical filtering.

To overcome these anomalies, we propose to map omnidirectional images on the sphere which is suitable for processing this kind of images. This mapping is performed using stereographic projection (see Fig.3 for an example).

Journal of Theoretical and Applied Information Technology
31st May 2013. Vol. 51 No.3

ISSN: 1992-8645 www.jatit.org E-ISSN: 1817-3195

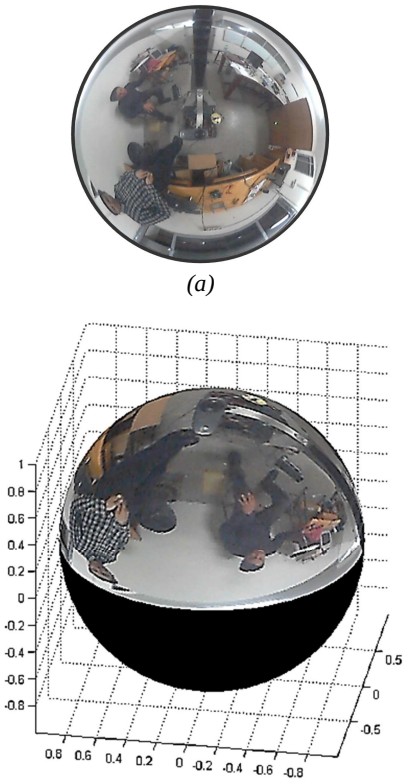

(a)

(b)

(c)

Figure 3. (a) Example of an omnidirectional image. (b) Omnidirectional image mapped on the sphere. (c) unwrapped panoramic image given for illustration

This choice is also mathematically valid, as it was demonstrated by Geyer and Daniilidis in [18] that most catadioptric omnidirectional images can be bijectively be mapped on the sphere. Considering a map from catadioptric image coordinates (u, v) to spherical coordinates (θ, φ) the catadioptric image $I(u, v)$ is mapped via inverse stereographic projection to $I_s(\theta, \varphi)$ on the sphere, then convolution with our developed SMCEV spherical kernels $G_s(\theta, \varphi)$ is performed directly on the sphere providing an output image $O(\theta, \varphi)$ which is stereographically projected to $O(u, v)$ on the plane (see Fig. 4).

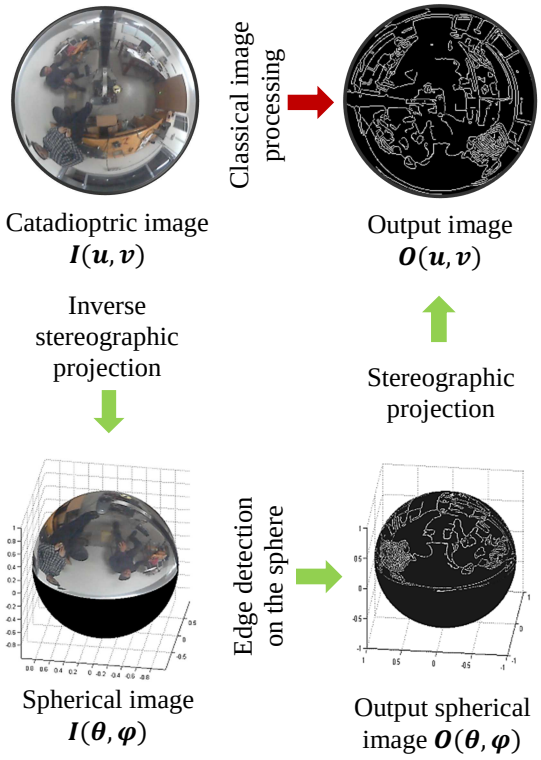

Figure 4. Omnidirectional image processing.

In Geometry, Stereographic projection is a method of representing the sphere onto a plane deprived of a point. It is often advisable that the deprived sphere point will be one of its poles. The projection plane may be that separates the two north and south hemispheres, called the equatorial plane. Stereographic projection can be made on any plane parallel to the equatorial one; in this case the projection plane would not contain the point which the sphere is deprived of. In our case the tangent plane on the North Pole is chosen as the projection plane.

In three-dimensional space $\mathbb{R}3$, the sphere is the set of points with three-dimensional vector such as:

$$P = (x_0, x_1, x_2)$$
$$= (r\cos\theta, r\sin\theta\sin\varphi, r\sin\theta\cos\varphi)$$

$$With\ r \in [0, \infty], \quad \theta \in [0, \pi] \quad and \quad \phi \in [0, 2\pi]$$

the stereographic projection is made from de south pole. It allows projecting any point of the sphere onto the tangent plane at the North Pole (see Fig. 5).

Journal of Theoretical and Applied Information Technology
31st May 2013. Vol. 51 No.3

ISSN: 1992-8645 www.jatit.org E-ISSN: 1817-3195

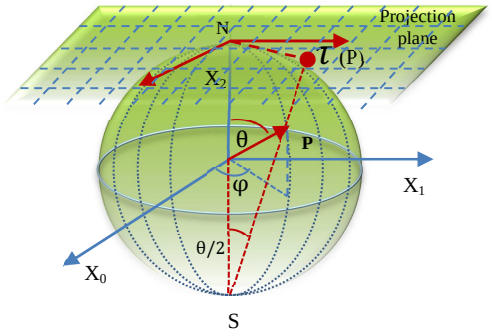

Figure 5 South polar stereographic projection.

If we take the sphere $S2$ as the Riemannian sphere $(r = 1)$ and the tangent plane as the complex plane $\mathbb{C}^2$, then the stereographic projection is a bijection given by:

$$\tau(p) = 2\tan\frac{\theta}{2}(\cos\varphi; \sin\varphi) \qquad (12)$$

Where $p = (\theta, \varphi)$, $\theta \in [0, \pi], \varphi \in [0, 2\pi]$

4. EXPERIMENTAL RESULTS

A series of experiments were done to evaluate the performance of the proposed approach. First a quantitative evaluation was conducted using a set of synthetic images (see Fig. 6a), in order to compare the behavior of the designed filter under noise, with some of most popular classical edge detection kernels. Sobel and Prewitt filters were chosen for being one of most studied edge extractors. Unlike some other methods, Sobel and Prewitt filters are more stable. The performance of Methods like Canny or Laplacian of Gaussian depends heavily on the optimization of their internal adjustable parameters such as the standard deviation Sigma, or high and low values of the threshold. So a compromise has to be made between noise filtering and accurate localization of the edge.
Experiments on real omnidirectional images are also presented in favor of judging the proposed filter performance in real conditions of use.

4.1 Quantitative assessment of edge detection performance:

In order to carry out the comparison between the studied edge detectors, we have chosen to quantify their performance using the Fram & Deutsch method presented in [32]. This method defines two quantitative measures P_1 and P_2. The first one reflects the distribution of the true detected edge points in contrast to false ones which result from noise along the edge. The second measure can be regarded as a maximum likelihood estimate of ratio of the total number of true edge points to the total number of detected edge points. P_1 and P_2 are equal to 1 for perfect edge detection. Their expressions may now be given. Let R be the edge detection output region taken into consideration (see Fig. 5b), containing R_{in} as the inside edge area and R_{out} as the outside edge area. Thus n_{tot} denotes the total number of points of R. n_{in} the number of points of R_{in}, and n_{out} the number of such points in R_{out} ($n_{tot} = n_{in} + n_{out}$). n^0 indicates the number of detected thresholded points in R_{out} and n^e the number of such points in R_{in}. Let w_1^e be the number of columns contained in R_{in} and w_1^{stan} the number of columns contained in R. Finally let n^r be the number of rows of R_{in} and w_2 the number of rows of R. The two parameters P1 and P2 are given by:

$$P_1 = \frac{n_{sig}^e}{n_{sig}^e + (n_{noise}^e + n^0)\frac{n_{in}}{f n_{tot}}} \qquad (13)$$

Where $n_{sig}^e = (n^e - n_{noise}^e)/1 - n_{noise}^e/n_{in}$

$n_{noise}^e = n^0 n_{in}/n_{out}$ and $f = {w_1^e}/{w_{stan}^e}$

$$p_2 = \frac{\frac{n_r}{w_2} - \left\{1 - \left[1 - \frac{n_{noise}^e}{n_{in}}\right]^{w_1^e}\right\}}{\left[1 - \frac{n_{noise}^e}{n_{in}}\right]^{w_1^e}} \qquad (14)$$

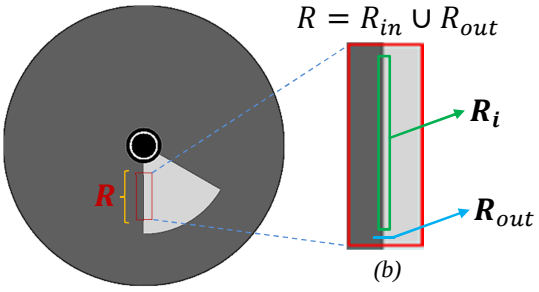

Figure 6. (a) Synthetic image used for the quantitative evaluation. With a vertical edge 0° and a diagonal edge 60°. (b) The considered edge region.

The set of synthetic images used to evaluate the proposed algorithm is composed of three artificial images with two kinds of edges, the first one is vertical, and the second is a diagonal edge with an

Journal of Theoretical and Applied Information Technology
31st May 2013. Vol. 51 No.3

ISSN: 1992-8645 www.jatit.org E-ISSN: 1817-3195

angle of 60°. The first image has a step of 50 gray levels between the two considered regions, the step of the second one is 100 and the third one is 150. A Gaussian noise with increasing variance σ is added initially to these images in order to evaluate the behavior of each studied filter. In order to implement the Fram & Deutsch evaluation method, a thresholding process is needed. The parameter P_1 is strongly correlated to the chosen value of the threshold, therefore we opted to select the threshold providing the best value of P_1 for every processed image. Classical Sobel, Prewitt and the planar Virtual Electrostatic Charge Model kernels abbreviated as PMCEV were performed on the planar omnidirectional images. While the Spherical Virtual Electrostatic Charge Model (SMCEV) developed in section 2 was applied on the spherical omnidirectional image as explained in section 3.

Charts below illustrate comparative robustness study of each filter against increasing Gaussian noise variance over vertical and diagonal edges.

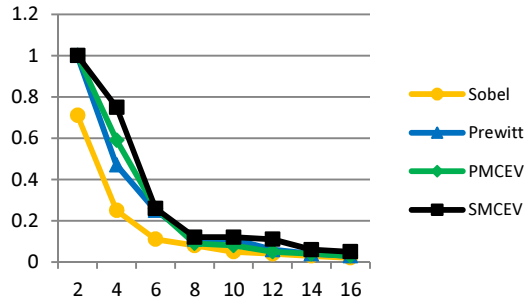

Figure 7. P_1 values on increasing Gaussian noise variance (vertical edge, 50 gray levels Step)

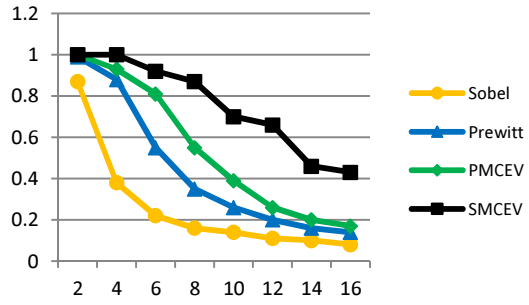

Figure 8. P_1 values on increasing Gaussian noise variance (vertical edge, 100 gray levels Step)

TABLE 1: P1 values on increasing Gaussian noise variance. (Vertical edge, 150 gray levels Step)

σ	2	4	6	8	10	12	14	16
Sobel	0,85	0,42	0,24	0,18	0,16	0,15	0,13	0,12
Prewitt	0,99	0,91	0,71	0,48	0,41	0,29	0,25	0,2
PMCEV	1	0,99	0,89	0,71	0,54	0,49	0,39	0,3
SMCEV	1	1	1	1	0,97	0,95	0,89	0,81

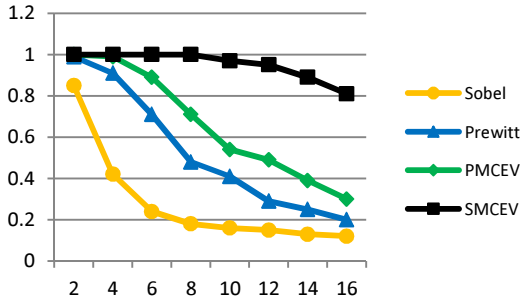

Figure 9. P1 values on increasing Gaussian noise variance (vertical edge, 150 gray levels Step)

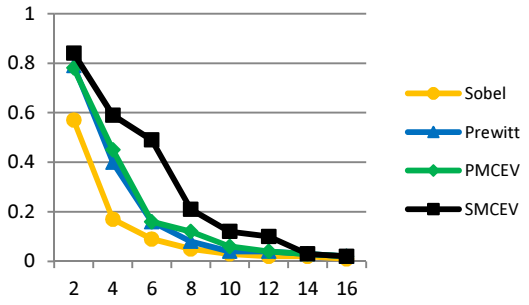

Figure 10. P_1 values on increasing Gaussian noise variance (Diagonal edge, 50 gray levels Step)

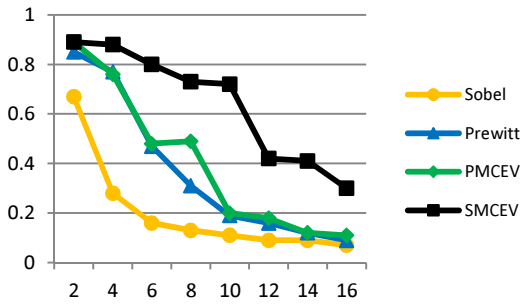

Figure 11. P_1 values on increasing Gaussian noise variance (Diagonal edge, 100 gray levels Step)

Journal of Theoretical and Applied Information Technology
31st May 2013. Vol. 51 No.3

ISSN: 1992-8645 www.jatit.org E-ISSN: 1817-3195

TABLE 2: P1 values on increasing Gaussian noise variance. (Diagonal edge, 150 gray levels Step)

σ	2	4	6	8	10	12	14	16
Sobel	0,61	0,32	0,21	0,15	0,13	0,11	0,1	0,09
Prewitt	0,72	0,71	0,51	0,39	0,33	0,23	0,2	0,18
PMCEV	0,85	0,81	0,59	0,41	0,33	0,26	0,21	0,16
SMCEV	0,88	0,88	0,87	0,87	0,86	0,78	0,71	0,65

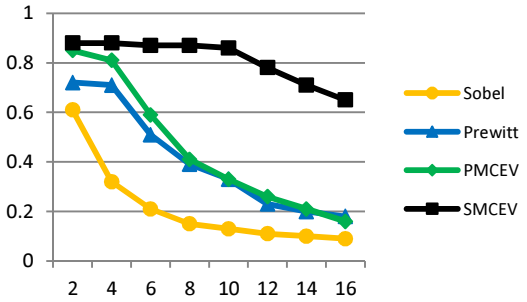

Figure 12. P_1 values on increasing Gaussian noise variance (Diagonal edge, 150 gray levels Step)

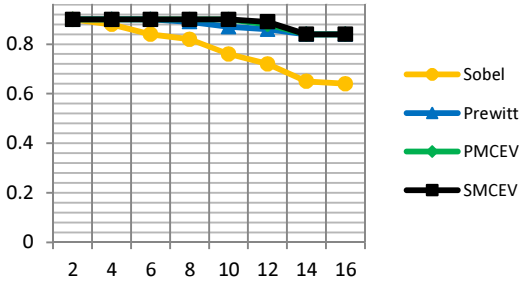

Figure 13. P_2 values on increasing Gaussian noise variance (Diagonal edge, 50 gray levels Step)

As P_1 illustrates the performance of each edge detection operators against noise, results above show that in both vertical and diagonal edge situations, the SMCEV approach is less affected by noise as it returns least false edges. It can be seen that Sobel operator provides worst results with considerable sensitivity to noise; its parameter P_1 begins to decrease notably at low Gaussian noise variance. While P_1 for PMCEV and Prewitt operators decreases more slightly than Sobel one. These findings are remarkably noticeable when the gray level step between the two considered regions increases; in this case the analysis is more discriminant.

The efficiency of all the studied edge detection operators degrades averagely while performing diagonal edges unlike vertical ones.

Considering the parameter P_2. The distribution of the output over the length of edges of the proposed approach is better than the compared methods as shown in figure 13.

We deduce that the proposed method furnish optimal edge detection outputs as it doesn't discard the resolution variation of omnidirectional images and respects the real positioning of neighboring pixels as it was illustrated in figure 3.

4.2. EXPERIMENTS ON REAL IMAGES

A checkerboard omnidirectional image presented in figure 14 has been considered to appreciate the behavior of the proposed edge detector in real conditions of use. Figures below show the results obtained with each detector.

Figure 14. Original real omnidirectional image of a Checkerboard.

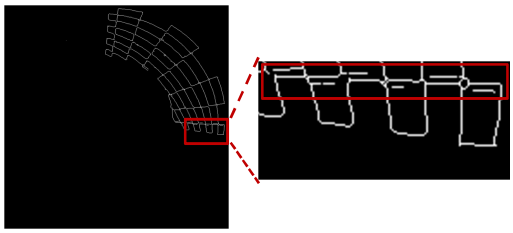

Figure 15. Omnidirectional image filtered with classical Sobel Operator.

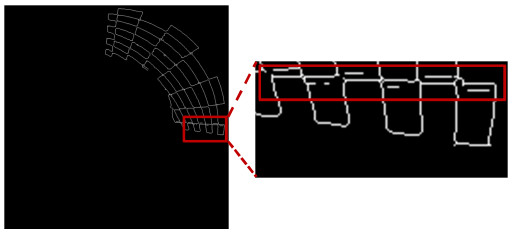

Figure 16. Omnidirectional image filtered with classical Prewitt Operator.

ISSN: 1992-8645 www.jatit.org E-ISSN: 1817-3195

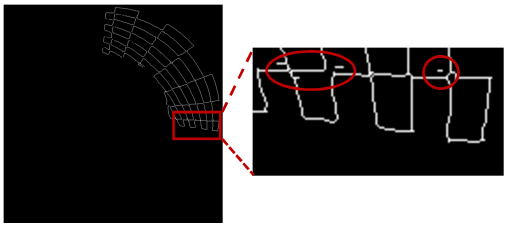

Figure 17. Omnidirectional image filtered with PMCEV Operator.

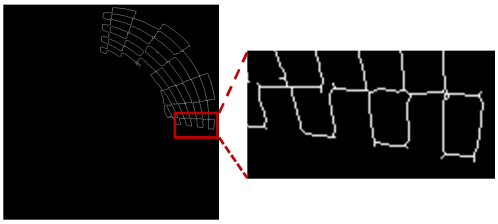

Figure 18. Omnidirectional image filtered with SMCEV Operator.

Figures 15-18 show that classical edge detectors tend to detect double edges in some regions of the real image. Conversely, our approach provides more reliable reproduction of real scene edges.

5. CONCLUSION

Omnidirectional images suffer from strong radial distortions and non-uniform sampling. Therefore, classical edge detection operators such as Prewitt and Sobel are not really suitable for this kind of images due to the failure of considering the correct neighboring pixels. Moreover all gradient-based edge detection methods are more sensitive to noise. We proposed a new edge detection approach specially adapted to omnidirectional images based on a virtual electrostatical model. On the one hand, this method has the advantage of respecting the geometrical properties of omnidirectional images. On the other hand, being non gradient-based, this approach improves edge detection robustness against noise, which was proved in the conducted quantitative evaluation study and also in the case of real conditions of use.

REFRENCES:

[1] H. Bakstein, T. Pajdla, Panoramic mosaicing with a 180◦ field of view lens, in: Proc. IEEEWorkshop on Omnidirectional Vision, Copenhagen, Denmark, June 2, 2002, pp. 60–67.

[2] Y. Xiong, K. Turkowski, Creating image based vr using a selfcalibrating fisheye lens, In CVPR97, pages 237--243, 1997.

[3] F. Kangni et R. Laganière, “Epipolar Geometry for the Rectification of Cubic Panoramas,” Third Canadian Conference on Computer and Robot Vision, CRV 2006.

[4] S. Peleg, M. Ban-Ezra, Stereo panorama with a single camera, in: Proc. IEEE Conf. Computer Vision and Pattern Recognition, June, 1999, pp. 395–401.

[5] R. Benosman et S. B. Kang, “Panoramic Vision : Sensors, theory and applications,” Ed Springer Verlag, 2001.

[6] P. Baker, C. Fermüller, Y. Aloimonos, R. Pless, A spherical eye from multiple cameras (makes better model of the world), in: Proc. Conf. on Computer Vision and Pattern Recognition, Vol. 1, Kauaii, USA, December, 2001, pp. 576–583.

[7]F. Kangni and R. Laganière, “Epipolar Geometry for the Rectification of Cubic Panoramas,” Third Canadian Conference on Computer and Robot Vision, CRV 2006.

[8] R. Cutler, Y. Rui, A. Gupta, J. Cadiz, I. Tashev, L. wei He, A.Colburn, Z. Zhang, Z. Liu, et S. Silverberg, “Distributed Meetings : A Meeting Capture and Broadcasting System” ACM Multimedia, 2002.

[9] T. Sato et N. Yokoya, “Omni-directional Multi-baseline Stereo without Similarity Measures,” IEEE Workshop on Omnidirectional Vision and Camera Networks (OMNIVIS 2005), October, 2005.

[10] S.K. Nayar, “Catadioptric omnidirectional camera”, IEEE Computer Society Conference on Computer Vision and Pattern Recognition, 1997, pp. 482-488.

[11] D.G. Aliaga, “Accurate catadioptric calibration for real-time pose estimation in room-size environments», *The 8th International Conference on Computer Vision*, 2001, pp. 127-134.

ISSN: 1992-8645 www.jatit.org E-ISSN: 1817-3195

[12] J. Baldwin and A. Basu, "3D estimation using panoramic stereo", *The 15th International Conference on Pattern Recognition,* 2000, pp. 97-100.

[13] J.P. Barreto and H. Araujo, "Geometric properties of central catadioptric line images", *The 7th European Conference on Computer Vision,* 2002, pp. 237-251.

[14] J.P. Barreto and H. Araujo, "Direct least square fitting of paracatadioptric line images", *CVPR2003 Workshop on Omnidirectional Vision and Camera Networks,*2003, pp. 78-83.

[15] E.L.L. Cabral, J.C. de Souza, and M.C. Hunold,"Omnidirectional stereo vision with a hyperbolic double lobed mirror", *The 17th International Conference on Pattern Recognition*, 2004, pp. 1-4.

[16] P. Doubek and T. Svoboda, "Reliable 3D reconstruction from a few catadioptric images", *The 3rd Workshop on Omnidirectional Vision*, 2002, pp. 71-78.

[17] C. Geyer and K. Daniilidis, "Catadioptric camera calibration", *The 7th International Conference on Computer Vision*, 1999, pp. 398-403.

[18] C. Geyer and K. Daniilidis, "Catadioptric projective geometry", *International Journal of Computer Vision*, 2001, Vol. 45, No. 3, pp. 223-243.

[19] C. Geyer and K. Daniilidis, "Paracatadioptric camera calibration", *IEEE Transactions on Pattern Analysis and Machine Intelligence*, 2002, Vol. 24, No. 5, pp. 687-695.

[20] C. Geyer and K. Daniilidis, "Properties of the catadioptric fundamental matrix", *The 7th European Conference on Computer Vision,* 2002, pp. 140-154.

[21] C. Geyer and K. Daniilidis, "Properties of the catadioptric fundamental matrix", *The 7th European Conference on Computer Vision,* 2002, pp. 140-154.

[22] T. Svoboda, T. Pajdla, and V. Hlavac, "Motion estimation using central panoramic cameras", *IEEE Conference on Intelligent Vehicles*, 1998, pp. 335-340.

[23] X.H. Ying and Z.Y. Hu, "Catadioptric camera calibration using geometric invariants", *IEEE Transactions on Pattern Analysis and Machine Intelligence*, 2004, Vol. 26, No. 10, pp.1260-1271.

[24] X.H. Ying and Z.Y. Hu, "Catadioptric line features detection using Hough transform", *The 17th International Conference on Pattern Recognition,* 2004, pp. 839-842

[25] Chen, C.-H., Yao, Y., Page, D., Abidi, B., Koschan, A., Abidi, M., 2003. Heterogeneous Fusion of Omnidirectional and PTZ Cameras for Multiple Object Tracking, IEEE Transactions on Circuits and Systems for Video Technology 18, p. 1052.

[26] Winters, N., Gaspar, J., Lacey, G., Santos-Victor, J., 2000. "Omni-directional vision for robot navigation," Proceedings of IEEE Workshop on Omnidirectional Vision, pp. 2128.

[27] Andreasson, H., Treptow, A., and Duckett, T., 2007. Self-localization in Non-stationary Environments using Omni-directional Vision, Robotics and Autonomous Systems 55, p. 541.

[28] Rituerto, A., Puig, L., Guerrero, J. J., 2010. "Comparison of omnidirectional and conventional monocular systems for visual slam," 10th Workshop on Omnidirectional Vision, Camera Networks and Non-classical Cameras, OMNIVIS 2010, Zaragoza, Spain.

[29] J. Cruz-Mota, I. Bogdanova, B. Paquier, M. Bierlaire, J.P. Thiran "Scale Invariant Feature Transform on the Sphere: Theory and Applications". International Journal of Computer Vision (10 November 2011), pp. 1-25.

[30] F. Jacquey, F. Comby, O. Strauss, "Fuzzy edge detection for omnidirectional images", Fuzzy Sets and Systems, Volume 159, Issue 15, 1 August 2008, Pages 1991-2010.

[31] B.Bouda, Lh. Masmoudi and D. Aboutajdine, "A new model for edge detection in digital images" ICGST, International Journal on Graphics Vision and Image Processing, Special Issu on edge detection and tracking, march 2006.

[32] J.R. Fram, E.S. Deutsch, "On the quantitative evaluation of edge detection schemes and their comparisons with human performance", IEEE Trans.Comput. C-24 (6) (1975) 616–627.